Pergamon

0038-1101(95)00364-9

Solid-State Electronics Vol. 40, Nos 1–8, pp. 785–798, 1996

0038-1101/96 $15.00 + 0.00

ORDERED ARRAYS OF QUANTUM DOTS: FORMATION, ELECTRONIC SPECTRA, RELAXATION PHENOMENA, LASING

N. N. LEDENTSOV[1]†, M. GRUNDMANN[1], N. KIRSTAEDTER[1], O. SCHMIDT[1], R. HEITZ[1], J. BÖHRER[1], D. BIMBERG[1], V. M. USTINOV[2], V. A. SHCHUKIN[2], A. YU. EGOROV[2], A. E. ZHUKOV[2], S. ZAITSEV[2], P. S. KOP'EV[2], Zh.I. ALFEROV[2], S. S. RUVIMOV[3]†, A. O. KOSOGOV[3]†, P. WERNER[3], U. GÖSELE[3] and J. HEYDENREICH[3]

[1]Institut für Festkörperphysik, Technische Universitat Berlin, Hardenbergstr. 36, D-10623 Berlin, Germany
[2]A. F. Ioffe Physical-Technical Institute, Politekhnicheskaya 26, 194021, St Petersburg, Russia
[3]Max-Planck-Institut für Mikrostrukturphysik, Weinberg 2, D-06120 Halle, Germany

Abstract—*Elastic relaxation on facet edges, renormalization* of the surface energy of the facets, and *interaction between islands via the strained substrate* are the driving forces for self-organization of *ordered arrays of uniform coherent three-dimensional islands* on crystal surfaces. For a (100) surface of a cubic crystal, two-dimensional square lattice of pyramid-like islands (quantum dots) with the periodicity along the directions of the lowest stiffness [010] and [001] has the minimum energy among different one-dimensional and two-dimensional arrays. For the InAs/GaAs(100) system, an *equilibrium* array of dots of the lateral size ~120–140 Å exists in a fixed range of growth parameters. The main luminescence peak at 1.1 eV, as well as peaks of excited states *coincide in energy with the peaks revealed in the calorimetric absorption spectra regardless* of the amount of InAs deposited (2–5 ML). Raman spectra indicate significant strain in InAs dots. The "phonon bottleneck" effect is bypassed via multi-phonon exciton and carrier relaxation. Ultranarrow lines (< 0.15 meV) are observed in cathodoluminescence spectra up to high temperatures. Low threshold current density operation via zero-dimensional states and ultrahigh temperature stability of the threshold current ($T_0 = 450$ K) are realized for a quantum dot injection laser. Increase in the gain and significant reduction in the radiative lifetime are possible via the self-organization of vertically-coupled quantum dots (VECODs) arranged in a well ordered *artificial three-dimensional tetragonal lattice.*

INTRODUCTION

The spontaneous formation of different ordered structures on crystal surfaces having a periodicity much larger than the lattice parameter was the subject of intense theoretical investigations[1–3]. More recently spontaneously formed nanostructures are considered as the most promising way of *in situ* fabrication of quantum wires and dots[4–8]. Severe modifications of electronic spectra, carrier relaxation and recombination mechanisms as well as drastic improvements in device characteristics are expected[9,10]. The ultimate limit is the fabrication of an ideal semiconductor atom-like quantum dot, having δ-function like energy levels. In order to realize fully the advantages of this approach one needs to create a dense and uniform array of wires or dots, otherwise inhomogeneous broadening can completely eliminate the advantages of reduced dimensionality. Nanostructures should have a size in a range of several nanometers to allow energy separation between electron and hole sublevels to be in the range of several kT at room temperature. Additionally they should be dislocation and defect free.

One mechanism of the formation of ordered nanostructures is faceting, where a planar crystal surface rearranges to a periodic hill-and-valley structure in order to decrease the surface free energy[1,2]. Faceting was experimentally observed, e.g. on Si and GaAs vicinal[11–13] and high-index surfaces[4,14], on low index Pt(100)[15], Ir(110)[16], TaC(110)[17]. Subsequent heteroepitaxial growth on faceted surfaces under optimized growth conditions may result in the formation of corrugated superlattices[4,12,18].

Another class of self-organized structures suitable for quantum wire and quantum dot fabrication is related to the spontaneous formation of ordered arrays of monolayer-high strained islands during submonolayer deposition of a material having large lattice mismatch with respect to the substrate[19,20]. Formation of ordered arrays of wire-like InAs islands oriented along [0–11] on GaAs (100) and vicinal surfaces has been observed by optical methods[19]

†On leave from the A. F. Ioffe Physical Technical Institute.

and directly by scanning tunnelling microscopy[20]. Periodic thickness modulation resulting in the formation of a quantum wire array oriented along the same [0–11] direction has been discovered in ultrathin InGaAs layers[21,22]. Recently, a metastable periodic corrugation resulting in an array of wires oriented along [001] has been demonstrated for 1–1.5 ML InAs deposited on a GaAs (100) surface[23]. For this class of nanostructures, the planar surface of the deposited material without external stress is stable against faceting. Under externally applied stress, caused by the lattice mismatch with the substrate, the planar surface becomes unstable against long-wavelength corrugation[24,25]. When the critical amount of strained material is deposited, this instability results in the formation of coherent strained islands on the bare substrate for Volmer–Weber (VW) growth or on the wetted surface for coherent Stranski–Krastanow (SK) growth. The formation of islands leads to a reduction of the strain energy and to an increase of the surface energy as compared to the planar case. The first is proportional to the volume of the island, and the latter is proportional to the surface area of the island. If the size of such an island exceeds a critical value, further growth becomes energetically favourable. It is generally assumed that if the material supply is interrupted, the further growth of large islands occurs at the expense of smaller islands, i.e. islands undergo ripening.

In this sense it comes as a surprise that, experiments show in most cases rather narrow size distribution of *three-dimensional* islands[6–8]. This is not an effect due to the SK or VW growth modes themselves. On top of that, the authors of Refs[8,22,23,26] have reported that coherent islands of InAs form, under certain conditions, a quasi-periodic square lattice. The lateral periodicity and the island size do not change with time. To explain the effects observed we have considered theoretically the possibility of spontaneous formation of an ordered array of strained coherent islands.

THEORY OF FORMATION

Important theoretical work has been carried out to describe elastic properties of different surface effects, steps, facets and the interaction between them[1–3]. Elastic relaxation due to *intrinsic surface stress*[2] at the facet edges has been considered. Particularly, the theory of elastic interaction for faceted surfaces developed by Marchenko[2] emphasized the role of intrinsic surface stress for the formation of equilibrium structure. The discontinuity of the surface stress tensor τ_{ij} at the facet edges results in effective forces F applied to the edges. These forces create a long-range strain field which yields a significant elastic relaxation. Contrary to the relaxation at a flat surface where the strains decay exponentially at the distance of a few lattice parameters, the edge-induced strain field decays only as L^{-1} with the distance from the edge. Thus the free energy of the faceted surface per unit area is equal to

$$E = E_{\text{FACETS}} + E_{\text{EDGES}} + \Delta E_{\text{EL}},$$

where E_{FACETS} is the surface free energy of the facets, E_{EDGES} is the short range contribution of the edges, the ΔE_{EL} is elastic relaxation energy due to edges. It was shown in Refs [1,2] that the free energy minimum corresponds to a periodic structure of facets, where E_{FACETS} does not depend on the period L, $E_{\text{EDGES}} \sim L^{-1}$, and $\Delta E_{\text{EL}} \sim L^{-1}\ln(L/a)$, where a is the cutoff parameter of the order of lattice spacing. The elastic relaxation energy per unit surface area always has a minimum for a particular size L^*, and the total free energy per unit area always has a minimum for the period L_0 which is determined by the interplay of E_{EDGES} and ΔE_{EL}.

We have considered several realistic shapes of strained islands[24]. First we establish that islands with well defined side facets and *no* planar top surface are more energetically favourable than islands with a flat top surface. This is mainly due to the fact that the material on the very top of the pyramid-like or ridge-like island is subject to the most efficient elastic relaxation of the volume strain.

Now we consider the energetics of an array of coherent islands under the constraint of fixed amount of deposited material Q assembled in all islands.

The change of the energy of the heterophase system due to formation of a single island, with respect to the uniformly strained flat epitaxial layer, is equal to

$$\Delta E_{\text{ISL}} = E_{\text{FACETS}} + E_{\text{EDGES}} + \Delta E_{\text{EL}}. \qquad (1)$$

E_{FACETS} is the extra energy of the tilted facets in comparison to their projection to the planar substrate. We consider the case where the (100) surface of the deposited material is stable; then the appearance of any tilted facet results in $E_{\text{FACETS}} > 0$. The second term in eqn (1), E_{EDGES}, is the short-range energy of edges. The third term, ΔE_{EL}, is the change of the strain energy due to elastic relaxation, called below "the elastic relaxation energy". For lattice-mismatched systems with edges, there are two sources of the strain field, namely the lattice mismatch ϵ_0 and the discontinuity of the intrinsic surface stress tensor τ_{ij} at the edges. Then ΔE_{EL} equals,

$$\Delta E_{\text{EL}} = \Delta E_{\text{EL}}^{(1)} + \Delta E_{\text{EL}}^{(2)} + \Delta E_{\text{EL}}^{(3)}, \qquad (2)$$

where $\Delta E_{\text{EL}}^{(1)}$ is the contribution of lattice mismatch to the elastic relaxation energy, proportional to L^3, $\Delta E_{\text{EL}}^{(2)}$ is the mismatch-induced renormalization of the surface energy, proportional to the surface of the island, and the third term, $\Delta E_{\text{EL}}^{(3)}$, is the contribution of edges to the elastic relaxation energy. $\Delta E_{\text{EL}}^{(3)}$ is proportional to $-L\ln\{L/(2\pi a)\}$. For islands of a size larger than the critical one, the first term in eqn (2) is the dominant contribution to ΔE_{EL}. We

assume that the surface energy of facets has a local cusped minima at low-energy facets $(k0l)$, $(kl0)$, $(k0\text{-}l)$ and $(k-l0)$, and we consider possible shapes of islands bound by these facets. These shapes include e.g. a pyramid with a square base and a prism with a rectangular base. Calculations show that the square-based pyramid is energetically more favourable than the elongated prism.

For a dilute system of islands, the elastic interaction between islands via the strained substrate may be neglected. Then, summing contributions of identical pyramid-shaped islands, one gets the energy of the dilute system of islands per unit area, $E_{\mathrm{DIL}} \cdot E_{\mathrm{DIL}}$ contains a term, which is the contribution of edges to the elastic relaxation energy, $\Delta E_{\mathrm{EL}}^{(2)} \sim L^{-2} \ln L$. It always has a minimum as a function of L. This may lead to a *total energy minimum at some optimum size of island L*. Thus, under some particular criterion, an equilibrium array of *equishaped* and *equisized* islands may be formed on the surface.

For a *dense* system of islands, the energy of the elastic interaction between islands via the strained substrate, E_{INTER}, becomes important. The minimum of the strain energy of different systems of stress domains usually corresponds to a *periodic domain structure*[27,28]. We show in Fig. 1(a) the sum of the energy $\Delta E_{\mathrm{EL}}^{(1)}$ and the interaction energy E_{INTER} for different two-dimensional periodic arrays of pyramids and for a one-dimensional periodic array of elongated prisms ("ridges"). It is seen from Fig. 1 that two-dimensional square and hexagonal arrays of islands are energetically more favourable than a one-dimensional array of quantum wires. Among the different arrays of pyramid-shaped islands on the (001) surface of the elastically anisotropic cubic medium, the minimum energy corresponds to the two-dimensional square lattice of islands with the main axes along the "soft" directions [010] and [001].

To study the dependence of the energy on the island size, it is convenient to introduce the characteristic length L_0

$$L_0 = 2\pi a \cdot \exp\left[\frac{f_4(\varphi_0)\eta\lambda}{f_3(\varphi_0)\tau^2} + \frac{1}{2}\right], \tag{3}$$

with η being the characteristic energy of the facet edge.
and the characteristic energy per unit area $E_0 = (Qa)\cdot(3\cot\varphi_0 f_3(\varphi_0))\,\tau^2\lambda^{-1}L_0^{-2}$.

Then the sum of all L-dependent terms in E reduces to [24]

$$E(L) = E_0\left[-2\left(\frac{L_0}{L}\right)^2 \cdot \ln\left(\frac{\sqrt{e}L}{L_0}\right) + \frac{4\beta}{e^{3/4}}\cdot\left(\frac{L_0}{L}\right)^{3/2} + \frac{2\alpha}{e^{1/2}}\cdot\left(\frac{L_0}{L}\right)\right]. \tag{4}$$

The function $E(L)$ is governed by two control parameters,

$$a = [\gamma(\varphi_0)\sec\varphi_0 - \gamma(0) - f_2(\varphi_0)\tau\epsilon_0]\frac{\sqrt{e}\lambda L_0}{f_3(\varphi_0)\tau^2},$$

$$\beta = (Qa)^{3/2}\cdot\frac{e^{3/4}f_5(\varphi_0)(6\cot\varphi_0)^{3/2}}{2f_3(\varphi_0)}\cdot\frac{(\lambda\epsilon_0)^2L_0^{1/2}}{\tau^2}. \tag{5}$$

α is the ratio of renormalized surface energy and the contribution of edges to the elastic relaxation energy of a single island, $\Delta E_{\mathrm{EL}}^{(2)}$. The parameter β is the ratio $E_{\mathrm{INTER}}/|\Delta E_{\mathrm{EL}}^{(2)}|$, φ_0 is the tilt angle of facets, $f_1, f_2, f_3, \ldots$ being functions of the tilt angle of facets[24] φ, and φ_0 is $\tan^{-1}(k/l)$. λ is a characteristic elastic modulus, ϵ_0 is the lattice mismatch, τ is the intrinsic surface stress, a is the lattice parameters, γ is the surface energy of tilted facets.

In Fig. 1(b) we show the phase diagram of the stability of the equilibrium array of quantum dots as a function of two control parameters α and β:

In Fig. 1(c) we show the total energy calculated for a system of weakly-interacting ($\beta = 0$) strained pyramid-like three-dimensional islands. The curves exhibit an energy minimum for a particular size of the dot; α in Fig. 1(c) equals: 0; 0.5; 1.1; 1.2; $2e^{-1/2} = 1.213$; 1.3, respectively.

For region 1 of the phase diagram of Fig. 1(b) there exists an optimum size $L = L_{\mathrm{opt}}$, corresponding to the absolute minimum of the energy, $\min E(L) = E(L_{\mathrm{opt}}) < 0$. The ripening of islands would correspond to $L \to \infty$ where the energy $E(L) \to 0$. This means that the two-dimensional periodic square lattice of islands having an optimal size L_{opt} is a *stable* array of islands which do not undergo ripening. In region 2 of the phase diagram, there exists only a local minimum of the energy, where $E(L') > 0$. In this case the array of islands having the size L' is a *metastable* array. For region 3, the local minimum in the energy $E(L)$ disappears. In both regions 2 and 3, there exists the thermodynamic tendency towards ripening. If the system initially corresponds to region 1, and the amount of the deposited material Q increases, the point in the phase diagram moves to region 2 or 3, and the array of coherent islands undergoes ripening. The physical reason for this is the repulsive interaction between islands via the strained substrate, which increases the total energy of the array of islands.

Due to renormalization of the surface energy of the facets caused by elastic relaxation of *volume* strain of the island, α can be of both signs. If $\alpha \leqslant 0$, there exists an absolute minimum of the energy $E(L)$ for any arbitrary value of β. Besides the absolute minimum of $E(L)$, there also exists a local minimum at $L = L'$, the energy of the corresponding metastable state $E(L') < 0$ in the region 4, $E(L') > 0$ in the region 5. No metastable state exists in region 6. According to the theory, a decrease of the lattice mismatch should

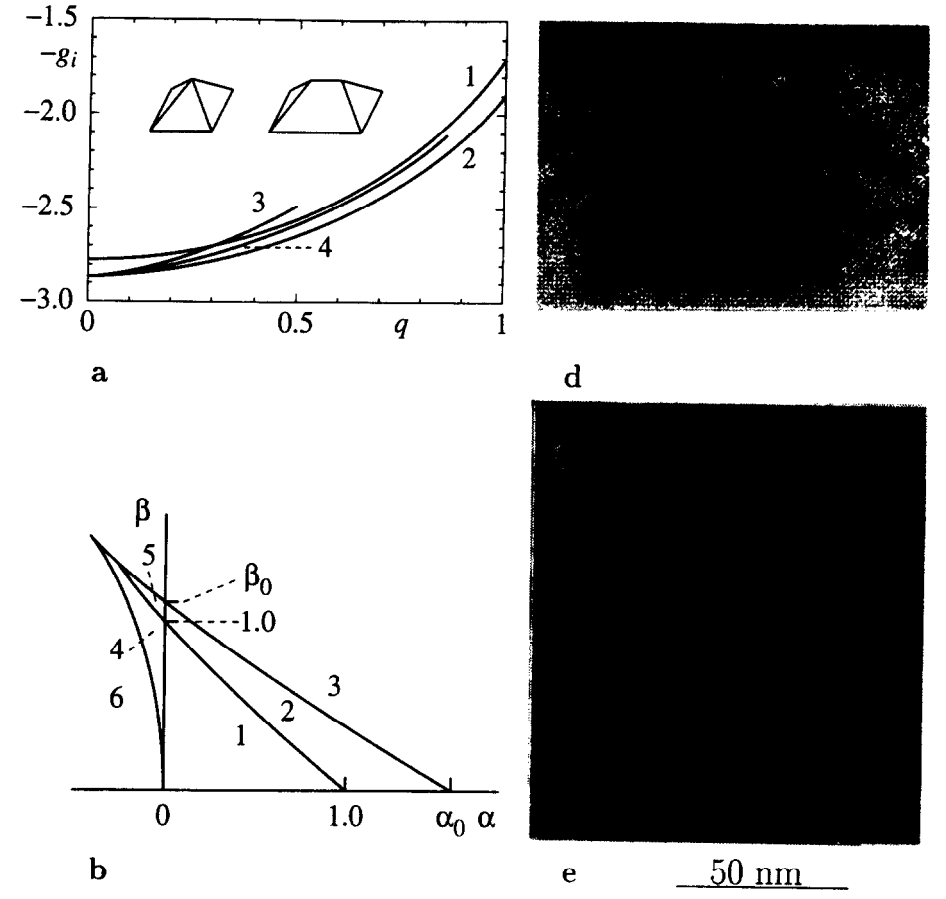

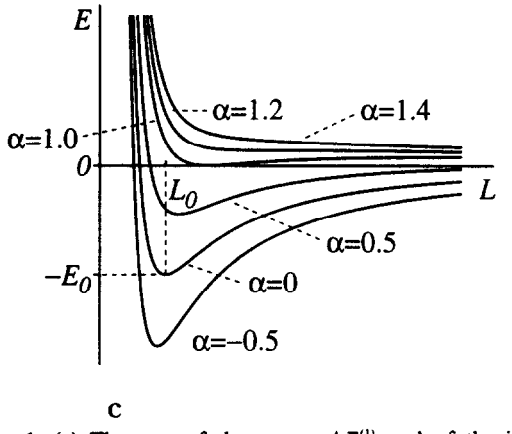

Fig. 1. (a) The sum of the energy $\Delta E_{EL}^{(1)}$ and of the island interaction energy E_{INTER} for different two-dimensional periodic arrays of coherent strained islands vs the fraction q of the surface covered by islands. (1)—one-dimensional array of prisms elongated in the [010] direction; (2)—two-dimensional square lattice of pyramids with primitive lattice vectors (1,0,0) and (0,1,0); (3)—two-dimensional checkerboard lattice of pyramids with primitive lattice vectors $(1,-1,0)$ and (1,1,0); (4)—two-dimensional hexagonal lattice of pyramids with primitive lattice vectors $(-1/2,-\sqrt{3}/2,0)$ and (1,0,0). Curves 3 and 4 terminate at maximum possible coverages for given arrays of islands. (b) Schematic phase diagram of the stability of square lattice of coherent strained islands in the plane of control parameters α, β. Here α is the ratio of the renormalized surface energy and of the contribution of edges to the elastic relaxation energy of a single island, $\Delta E_{EL}^{(2)}$. The parameter β is the ratio $E_{INTER}/|\Delta E_{EL}^{(2)}|$, it increases with the amount of the deposited material as $Q^{3/2}$. In regions 1, 4, 5 and 6, there exist stable arrays of islands which do not undergo ripening. In regions 2 and 3 islands always undergo ripening. (c) The total energy E for a system of weakly-interacting strained pyramid-like three-dimensional islands. Calculations of E include strain relaxation on the edges of the pyramids and renormalization of the surface energy of facets. (d) Cross-section and plan-view. (e) Transmission electron microscopy images of InAs-GaAs quantum dots formed by 5 Å InAs–15 Å GaAs–5 Å InAs–15 Å GaAs–5 Å InAs-deposition. An artificial tetragonal lattice composed of laterally ordered and vertically-coupled quantum dots locally distorted by statistical fluctuations is formed.

result in an increase of the lateral size and in the decrease of the tilt angle of facets, if all the other parameters are the same. An increase of the surface energy of facets should lead to similar results.

In summary, there are two main reasons for the ordering of three-dimensional islands in size: elastic relaxation on facet edges and *renormalization of the surface energy of the facets*, caused by the relaxation of the *volume* strain of the islands. The latter effect can significantly reduce the energy per unit surface area as compared to the pseudomorphic layer case. A periodic array of coherent islands of the same optimal size corresponds, under certain conditions, to the minimum of the total energy. This is in an agreement with recent experimental observations[8,22–24,26].

The tendency for having a pyramid like shape and size ordering is important for free-standing islands. If the deposition rate during regrowth is fast enough the pyramid-like shape is maintained. On the contrary, e.g. for the InAs-GaAs case, if the InAs dot is only *partly* regrown with GaAs and another InAs deposition cycle is introduced, the InAs-GaAs superlattice arrangement becomes energetically favourable and each dot spontaneously splits on two InAs parts separated by a ~2–4 monolayer thick GaAs layer. The process can be continued resulting in laterally-periodic vertically-coupled quantum dots. An artificial three-dimensional tetragonal lattice is formed. Cross-section and plan-view TEM images of this structure formed by 5 Å InAs–15 Å GaAs–5 Å InAs–15 Å GaAs–5 Å InAs-deposition are shown in Fig. 1(d) and (e), respectively.

GROWTH AND CHARACTERIZATION

All samples were grown by elemental source molecular beam epitaxy (MBE) on GaAs (100) substrates using RIBER-32 and EP1203 MBE machines. Growth rates were 0.8 μm h^{-1} for GaAs and 0.3 μm h^{-1} for InAs. Arsenic pressure, substrate temperature during InAs deposition, and growth interruption time between submonolayer InAs deposition cycles were varied. After oxide desorption, a 0.5 μm-thick GaAs buffer was grown at 600°C, then 200 Å of $Al_{0.3}Ga_{0.7}As$ was deposited, followed by a 20 Å/20 Å GaAs-$Al_{0.3}Ga_{0.7}As$ superlattice (5 periods) and a 70–1000 Å GaAs layer. Then the substrate temperature was lowered to 450–520°C and the desired amount of InAs was deposited. Afterwards 50–100 Å of GaAs was grown at low temperature, then the substrate temperature was increased to 600°C and a 20 Å-thick GaAs layer was grown. This layer was followed by a 20 Å/20 Å GaAs-$Al_{0.3}Ga_{0.7}As$ superlattice (5 periods) and 200 Å of $Al_{0.3}Ga_{0.7}As$; a 50 Å GaAs layer was grown on top for surface protection. Reflection high-energy electron diffraction (RHEED) patterns were monitored during the growth. Formation of dots started after the deposition of a ~4.5 Å thick InAs layer and led to the transformation of a streaky RHEED pattern to a dashed one. Further InAs deposition resulted in well-developed diffraction spots typical for three-dimensional growth mode. Average thickness t_{av} of InAs deposited was varied between 1 and 15 Å.

Transmission electron microscopy (TEM) studies were performed using a high voltage JEOL JEM1000 (1 MV) microscope. The samples were chemically polished for plan-view TEM. TEM images were taken under conditions far away from the exact Bragg reflection to exclude the island shape modification by strain fields. Photoluminescence (PL) was excited using the 514.5 nm line of an Ar^+-ion laser and detected using a cooled germanium *pin*-photodetector. Excitation density was varied in the range of 0.01–500 W cm^{-2}.

InAs-GaAs STRUCTURES FORMED BY SUBMONOLAYER AND MONOLAYER InAs DEPOSITIONS

Submonolayer InAs deposition results in the formation of InAs wire-like one-monolayer high islands[19] having a uniform width of ~40 Å[20] oriented along the [0-11] direction. The island length-to-width ratio increases with the increase of the total amount of InAs deposited. Such an array of islands may be considered as a quantum wire or quantum dot array, depending on the fraction of monolayer covered with InAs. Resulting regrown structures exhibit excellent luminescence properties, ultranarrow PL and PL excitation (PLE) linewidths (down to 0.15 meV)[29] and high exciton oscillator strength (radiative lifetime ~60 ps) with practically no dependence on the average thickness of InAs deposited (0.08–0.9 ML)[30]. In Fig. 2 we show a plan view TEM image and PL spectra at 8 K at different excitation densities of a 1 Å InAs sample. Weak modulation of the contrast can be resolved in the TEM image. The stripes have a width of ~50 Å and are oriented along the [0-11] direction. PL spectra are dominated by three peaks: one due to the GaAs barrier free electron to acceptor transition, another due to GaAs free exciton recombination, the third one is due to excitons localized by InAs islands (E^{InAs}). The remarkable feature of Fig. 2 is the absence of broadening of the InAs bound exciton line with increase of the excitation density. The half-width at half maximum (HWHM) measured on the high energy side of the E^{InAs} line is close to ~0.7 meV for all excitation densities up to 500 W cm^{-2}, while the GaAs emission is dramatically broadened by many-body effects. This effect is in agreement with the quasi-zero-dimensional nature of InAs induced states.

Increase in the average thickness of InAs (1–1.5 ML) results in a change of the symmetry and of the period of the wire-like surface structure. For these thicknesses, the energy benefit due to strain relaxation via island formation cannot overcome the energy loss due to surface area increase, however,

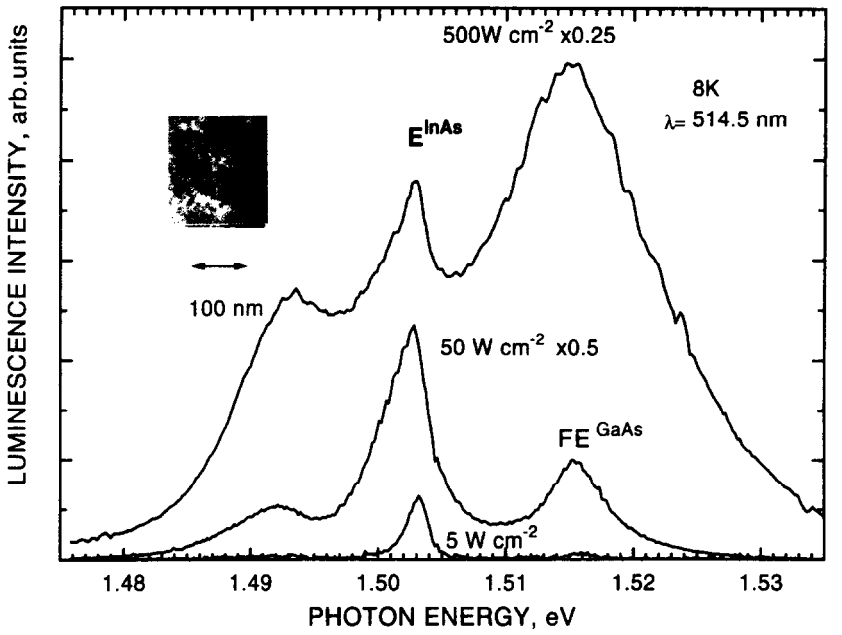

Fig. 2. Photoluminescence (PL) spectra at different excitation densities of 0.3 ML InAs in GaAs matrix. Plan-view TEM image is shown in the insert.

partial elastic strain relaxation may occur via long-wavelength corrugation of the InAs layer. A characteristic width of InAs wires oriented along [001] direction is close in this case to 200 Å[23]. Such a structure is metastable, at very long growth interruption times it flattens and then converts to an array of islands which is typical to the stage of submonolayer deposition and, additionally, multimonolayer InAs islands oriented along [0-11] direction[31].

The reason for the change of the direction of surface anisotropy may be qualitatively explained as follows. For low concentrations of InAs islands, the island shape anisotropy is defined by the anisotropy of the intrinsic surface stress tensor, which then reflects the symmetry of the surface reconstruction ([0-11] and [011] directions). When the surface is completely covered with InAs and the transformation to dots is not yet possible (the critical thickness of ~1.6–1.7 ML InAs is not yet reached), the bulk effects of the strain penetration to the GaAs substrate dominate. The orientation of the corrugation is then defined by [001] and [010] directions, which are the directions of lowest stiffness.

FORMATION OF InAs QUANTUM DOTS

After the critical average thickness of InAs deposition is reached (1.6–1.7 ML), morphological transformation to three-dimensional InAs islands occurs.

In Fig. 3, we show PL spectra and plan-view TEM images of the samples with 2 ML (a,c) and 4 ML InAs (b) deposited at 480°C with standard $\sim 2.10^{-6}$ torr arsenic pressure (P_{As}). No growth interruptions were introduced in cases (a) and (b). Sample (c) was deposited with submonolayer (0.3 ML InAs) growth cycles separated by 100 s long growth interruptions. Dots formed after the critical layer thickness is just exceeded are small, mostly do not show well resolved crystalline shape and exhibit large size dispersion. TEM contrast modulation with stripes along the [001] direction resembles the pretransformational InAs layer morphology (see above and Ref.[23]) and indicates that the wetting layer is modulated in thickness. Similar effects have been reported for InGaAs-GaAs growth while the wires were oriented along the [0-11] direction[8,21,22,32] in that case. Increase to 4 ML of the amount of InAs deposited results in a dense array of well-developed dots having a size of ~140 Å. The sides of the square-shaped base of the dot are parallel to either the [001] or [010] directions. The smaller size of the dots in the case of the 2 ML sample agrees well with a strong shift of the corresponding PL line towards higher photon energies.

Since the shape of the dot is different for 2 and for 4 ML InAs depositions one might question the existence of an *equilibrium shape of the dots*. We have found that the introduction of growth interruption 40 s (10 s) after the InAs is deposited is enough to let the dot reach its equilibrium size for 2.5 ML (3 ML) InAs deposition. Large clusters and dislocations do not appear in this case. With very long growth interruptions (sample c) one can even force $t_{av} = 2$ ML dots to reach equilibrium size. For this interruption time (10 min total) the wetting layer starts to decompose[31], resulting in the appearance of large clusters. However, the size of the dot approaches the equilibrium size [see Fig. 3(c)] and the PL peak coincides in energy with 4 ML InAs PL peak at ~1.1 eV. Thus, the growth interruption

experiments confirm the equilibrium nature of the dot array.

STABILITY OF THE EQUILIBRIUM DOT ARRAY

Changes of MBE growth conditions may result in modifications of surface reconstruction and, thus, may lead to a change of the facet surface energy. Since the stability of the equilibrium dot array strongly depends on the facet surface energy [see Fig. 1(b)] we can expect that a significant change in growth parameters influences the stability of the dot array. In Fig. 4, we visualize the arsenic pressure dependence of dot formation and of PL spectra (4 ML InAs, no growth interruptions). Standard MBE arsenic pressure [$P^0_{As} \sim 2.10^{-6}$ torr, 480°C, Fig. 4(c)] results in equilibrium dots of high density ($\sim 5 \cdot 10^{10}\,cm^{-2}$). The dot array is stable when the arsenic pressure is changed by ~50% around this value. An increase in As pressure by a factor of 3 ($3P^0_{As}$) results in dramatic changes of the growth mode [Fig. 4(d)]. The size of the dots reduces dramatically and a high concentration of large (~500–1000 Å) relaxed InAs clusters appears[33]. Accordingly the PL peak shifts towards shorter wavelengths due to increased carrier confinement energies in small coherent InAs dots. Further increase in arsenic pressure [5 P^0_{As}, Fig. 4(e)] even completely suppresses the dot formation and only macroscopic InAs clusters can be resolved on the featureless InAs wetting layer. PL emission is dominated by the wetting layer (~1.5 ML InAs) peak at low temperatures and no dot emission may be resolved at 300 K.

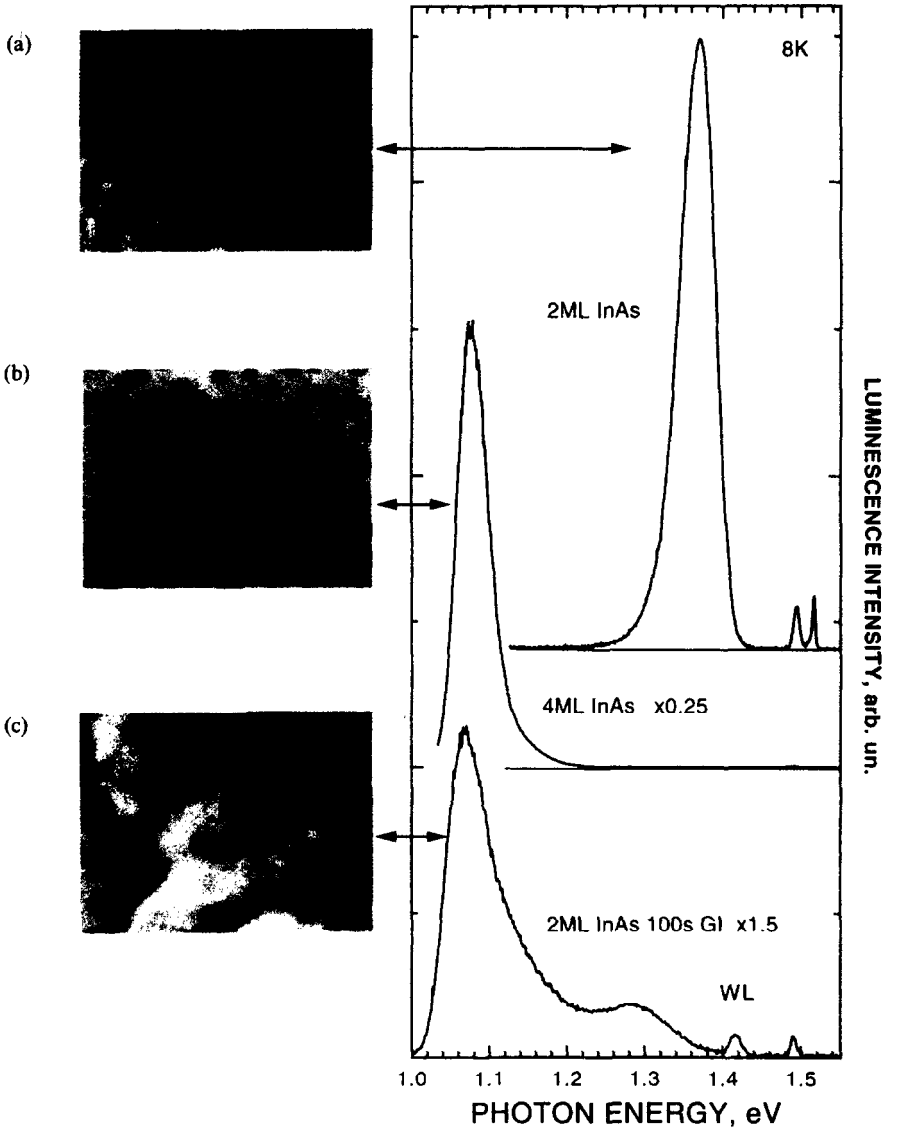

Fig. 3. PL spectra and plan-view transmission electron microscopy (TEM) images of structures with 2 ML (a,c) and 4 ML InAs (b) deposited at 480°C with standard ~2.10^{-6} torr arsenic pressure (P_{As}). No growth interruptions were introduced in cases (a) and (b). Sample (c) was deposited with submonolayer (0.3 ML InAs) growth cycles separated by 100 s long growth interruptions.

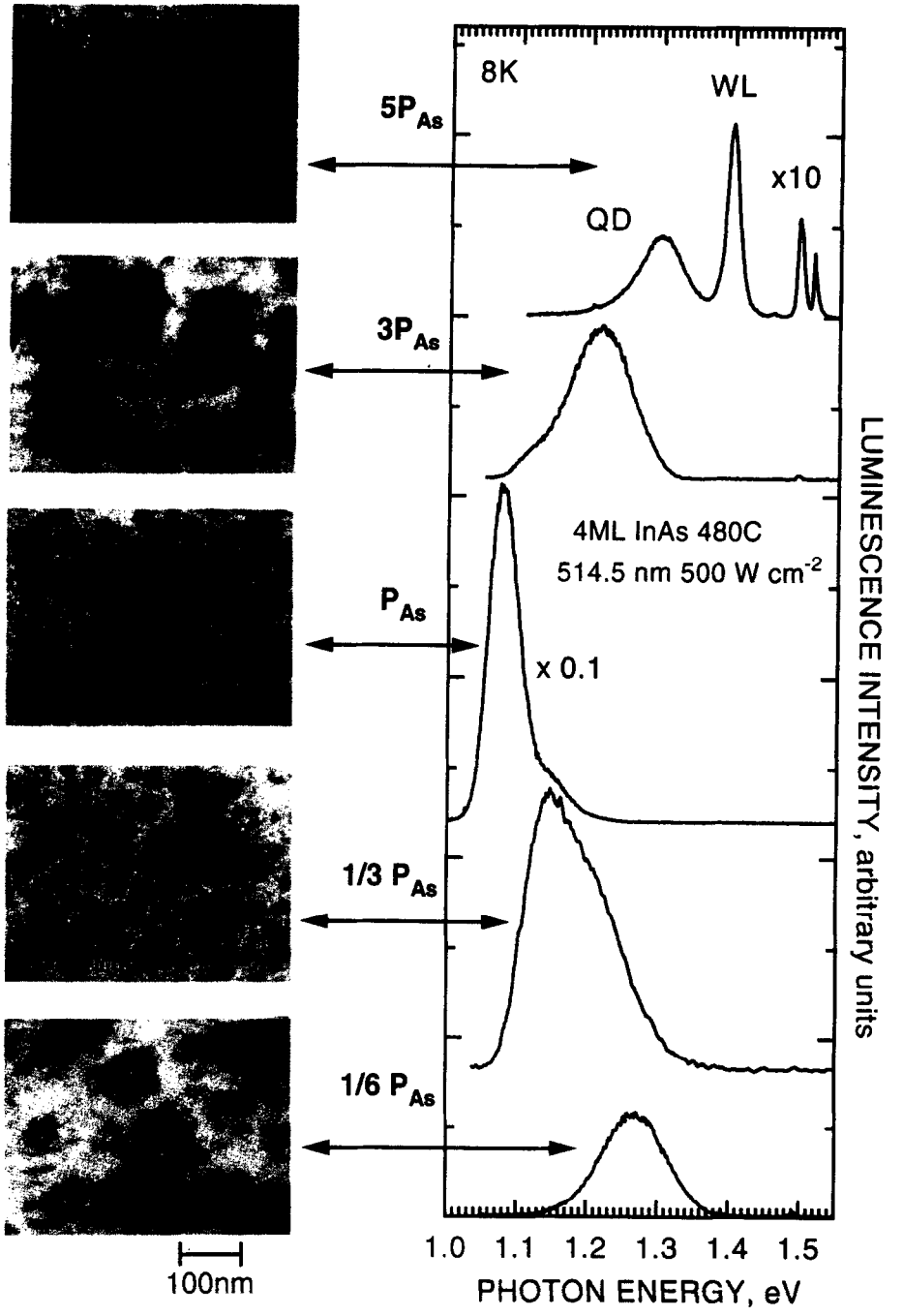

Fig. 4. Plan-view TEM images and PL spectra of the structures illustrating the influence of the arsenic pressure on dot formation (4 ML InAs). Both high and low arsenic pressures suppress the dot formation, however, mesoscopic three-dimensional InAs clusters are formed only at high arsenic pressure. PL degrades significantly both at low and high arsenic pressures.

The integral intensity of PL strongly degrades in agreement with the formation of large relaxed (dislocated) islands.

Reduction of arsenic pressure influences the dots in a different way. As shown in Fig. 4(b) (1/3 P^0_{As}), the dots undergo local "melting" and macroscopic two-dimensional InAs islands appear. The lateral size of the remaining dots is weakly affected. Further reduction in arsenic pressure [1/6 P^0_{As}, Fig. 4(a)] results in practically a complete disappearance of the dots in favour of macroscopic two-dimensional InAs islands. For these growth conditions which are close to "virtual surfactant epitaxy"[34], the RHEED pattern is streaky. No macroscopic three-dimensional InAs clusters are formed in this case. The PL peak shifts towards higher energies and broadens as the InAs arrangement resembles a highly nonuniform corrugated two-dimensional layer. However, the integral PL intensity strongly drops, as it was the case for the growth at high As pressure.

We emphasize that *both low and high arsenic pressures* result in *macroscopic surface structures* (~1000 Å). For the highest arsenic pressure, InAs clusters are separated by 0.2–1 μm. This indicates that *growth kinetics* do not play any important role, particularly not for equilibrium dots having a size of ~120–140 Å and a typical separation of 250–350 Å. Moreover, we have found that the RHEED pattern converts from spotty to streaky within several seconds if the As flux is interrupted and 0.15 ML of pure indium is deposited even *after* the three-dimensional dots are formed (4 ML InAs deposition under the optimal As pressure).

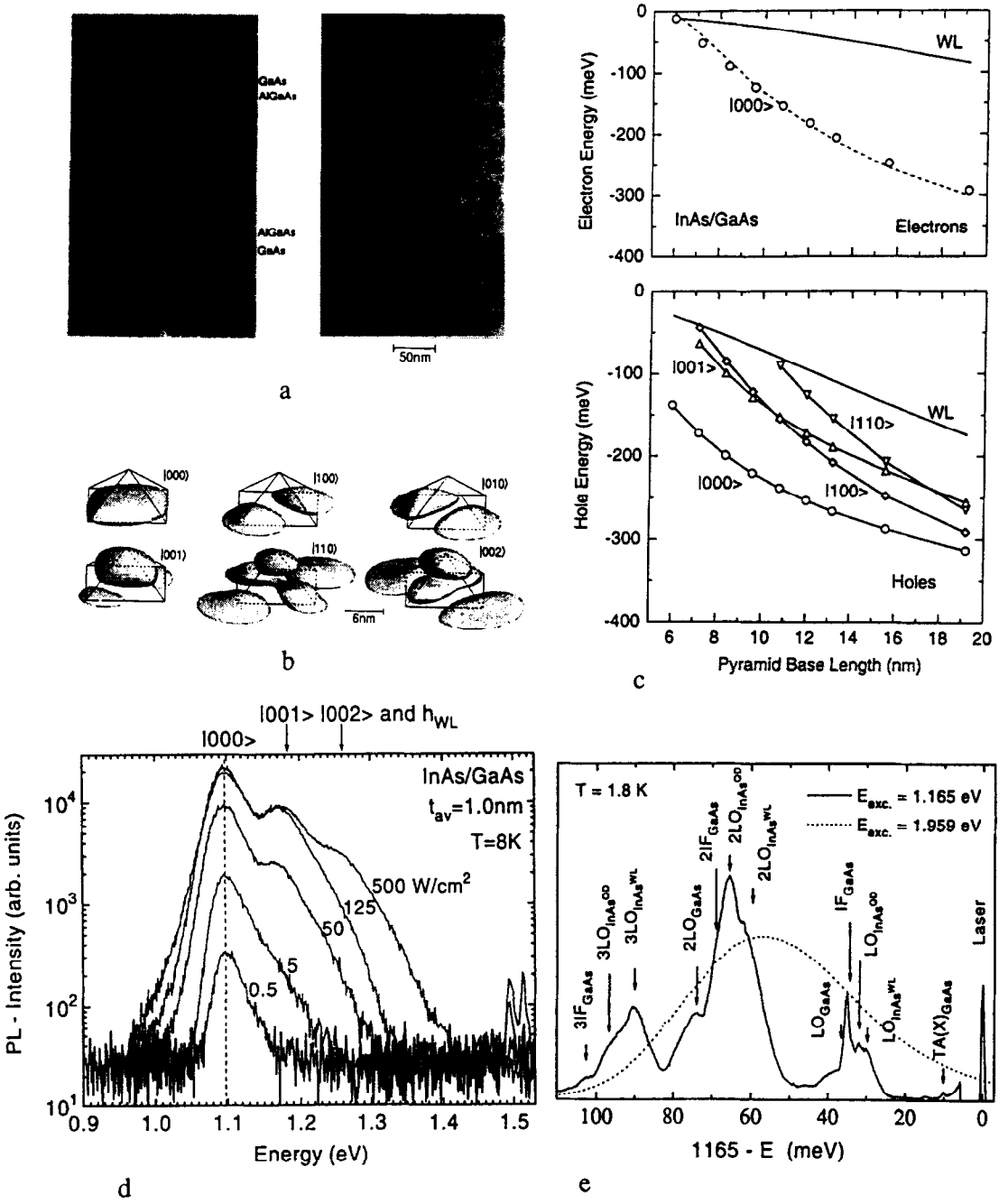

Fig. 5. (a) High-resolution cross-section electron microscopy image (left) of InAs dots viewed along [001] direction and plan view TEM image, local ordering in two-dimensional lattice may be resolved. (b) Ground and excited hole state wavefunctions in 12 nm base side quantum pyramid. (c) Calculated energy levels of ground electron state and ground and excited hole states as a function of a quantum pyramid base side. (d) PL spectra at 8 K of 3 ML InAs quantum dots for different excitation densities given in W cm^{-2}. Predicted transition energies of excited hole levels are indicated. (e) Luminescence spectra of InAs quantum dots excited at 1.165 eV (full line) and 1.959 eV (dashed line). The energies are given with respect to the 1.165 eV excitation line. Note broad overlapping resonances with energies characteristic to different InAs and GaAs-related phonons and their multiples.

An increase of substrate temperature from 480°C to 520°C keeping the arsenic pressure at P^0_{As} results in an increase of the lateral size of the dot to ~180 Å and in a strong decrease of dot density (down to $\sim 1.5\text{–}2 \cdot 10^{10}\,cm^{-2}$). The dot lateral shape (well-defined square) is not affected. Large clusters appear locally. PL peak position shifts slightly (~30–50 meV) towards higher energy with respect to the PL line for 480°C growth, indicating that the increase of the lateral size is compensated by the reduction of the dot height and the facet angle.

ELECTRONIC SPECTRUM

In order to analyze the electronic spectrum one needs to define precisely the equilibrium dot geometry in all directions. In Fig. 5(a) we show high-resolution cross-section (along the [001] direction) and high-voltage plan-view TEM images of an *ordered array* of InAs dots. Local ordering of dots can be observed. The lateral size of the dot is close to 120–130 Å in this case and the height is ~60 Å. The dots have a well-defined pyramid-like shape and are arranged in a two-dimensional square lattice distorted by statistical fluctuations [see also Fig. 1(e)]. A short-period GaAs-AlGaAs superlattice below and above the dot layer in 140 Å GaAs is also clearly resolved. We note that a planar surface is completely re-established after only 70 Å GaAs regrowth. Detailed theoretical calculations of strain distribution and electronic structure of pyramid-like InAs quantum dot with {101}-like side facets including piezoelectric and excitonic effects have been carried out[35]. Results show that only one electron, but several hole states, exist in a pyramid-like dot of such size. Only $|3/2, 3/2\rangle$ hole states play a role. Figure 5(b) displays the ground state (GS) and excited hole state wavefunctions in a 12 nm base quantum pyramid and Fig. 5(c) displays the ground state electron and the ground state and excited state hole energies as a function of base size. The hole ground state (GS) has an overlap of 88% with the electron GS. Contrary to the case of rectangular box-like QDs, excited $|001\rangle$ ($|002\rangle$) hole states have a large overlap of 34% (11%) with the electron GS and thus induce an allowed transition. A finite small overlap of $|100\rangle$ (<0.01%), $|010\rangle$ (0.5%) and $|110\rangle$ (2.5%) hole states is due to piezoelectric effects at {112}-like facet edges. The exciton binding energy is close to 20 meV, i.e. more than one order of magnitude larger than in the bulk InAs[35].

PL spectra for different excitation densities of an ordered dot array are shown in Fig. 5(d). PL spectra are dominated by the 40–50 meV broad GS PL line. Its intensity saturates at high excitation densities, where transitions between ground electron and excited ($|001\rangle$ and $|002\rangle$) hole states appear. All three transitions and also the wetting layer transition are observed at the same energies in calorimetric absorption spectra of the structures studied[8,36]. The calculated peak positions shown by arrows are found to agree quite well with those experimentally observed. The GS PL peak width (40 meV) corresponds to ~10 Å change in lateral size. This means that the lateral size of the dot fluctuates on average only within ±2 ML.

Excited hole states appear in PL spectra only at high excitation densities where the GS transition is saturated. This indicates that the intradot exciton relaxation occurs on a very fast time scale. Carrier capture time into QDs was estimated by us to be close to 1 ps[37]. Severe limitations (capture time of ~100 ps) arise, however, for carrier capture into small InAs dots formed on the initial stage of dot formation [see Fig. 3(a)][38]. The radiative lifetime of the equilibrium GS QD exciton is close to ~1.5 ns for dots having a lateral size of ~80–120 Å. Very small dots (~60 Å) show smaller lifetimes due to the expansion of the exciton wavefunction into the GaAs barrier regions (Rashba effect)[39]. The radiative lifetime of 1.5 ns is comparable to radiative lifetime of bound exciton complexes in GaAs which have though a much larger effective exciton volume. Thus the QD oscillator strength per unit exciton volume is dramatically increased by approximately two orders of magnitude in agreement with the strongly increased exciton binding energy. The saturation of the *integral* PL intensity of dense dot arrays observed for very high excitation densities indicates an efficient channel of nonradiative recombination connected with a high concentration of nonequilibrium carriers, probably Auger recombination via occupied excited hole levels.

Under highly spatially resolved excitation with a focused electron beam, the luminescence spectrum consists of a series of ultranarrow (FWHM < 0.15 meV) lines, each originating from a single InAs quantum dot[8,26,36]. The *lines do not exhibit broadening with temperature increase*, which indicates directly an atom-like electronic spectrum of a single dot[26,36].

Figure 5(e) displays the PL spectra of QDs under resonant (below GaAs quantum well bandgap, 1.165 eV) and non-resonant excitation (above the GaAs QW bandgap). Under resonant excitation the QD PL spectrum is dominated by several relatively broad (FWHM ~5–15 meV) peaks. The spectral intensity distribution of different peaks corresponds approximately to the PL lineshape under non-resonant excitation. The energies of the peaks agree with different types of InAs and GaAs-related phonons, including an interface GaAs phonon (34 meV), a bulk-like GaAs phonon (36.6 meV), an InAs wetting layer phonon (29.5 meV[40]), an InAs QD phonon (31.9 meV) and their multiples. When the photon energy of excitation is tuned by 90–100 meV above the GS transition energy, the phonon-related peaks broaden and finally merge

giving the shape characteristic to non-resonant excitation. A multi-peak structure with the same characteristic energies is revealed in PLE with InAs QD LO peaks dominating the spectra. The peaks may be attributed to resonant multi-phonon exciton relaxation between ground and excited exciton states. Higher order transitions involving 4 to 5 QD LO peaks are contributed by quasi-continuum and wetting layer hole states. The probability of recombining radiatively via GS is higher if the energy separation between the ground and excited states is resonant to one or several LO phonons. High integral intensity, PL decay times and the absence of other (thermalized) PL indicates that the structure represents rather resonant luminescence than resonant Raman scattering[41–46].

The importance of resonant LO-phonons for efficient carrier and exciton relaxation between the ground and excited states in a quantum dot has been demonstrated[8,47,48]. Here we found remarkable broadening and high integral intensity of phonon-related resonances in the case of relatively small (120–140 Å) quantum dots. Strong lateral localization of the exciton wavefunction makes possible efficient interaction with optical and interface phonons at all points of the Brillouin zone[49]. Moreover, remarkably large widths of the peaks exceed significantly the LO-phonon dispersion curves indicating additional broadening mechanism. This agrees with the fact that the exciton interaction with acoustic phonons at $k \neq 0$ with a large energy dispersion is also strongly enhanced[50]. The broadening mechanisms[51] together with the multi-phonon nature of the exciton relaxation make it possible to bypass the phonon-bottleneck effect in this case[8]. It is important to note that the energy of the InAs QD phonon (31.9 meV) is larger than the energy of the InAs bulk-like phonon (29.9 meV). This increase in the phonon energy equal to 32.1 meV agrees well with the calculation of the strain and of strain-induced changes in the InAs LO-phonon energy in coherent InAs quantum dots of pyramidal shape[35].

INJECTION LASING VIA ZERO-DIMENSIONAL STATES

Quantum dot lasers are expected to have superior properties with respect to conventional QW lasers. High differential gain, ultralow threshold current density and high temperature stability of threshold current density are expected to occur simultaneously[9,10]. Additionally, ordered arrays of scatterers formed in an optical waveguide region may result in the distributed feedback and (or) in the stabilization of single-mode lasing. Intrinsically buried quantum dot structures spatially localize carriers and prevent them from recombining nonradiatively on resonator facets. The overheating of facets, being one of the most important problems for high-power and high efficiency operation of GaAs-AlGaAs and InGaAs-AlGaAs lasers, may thus be avoided.

In this work, injection lasing via zero-dimensional states is observed for small (~80 Å) quantum dots formed by a 5 Å InAs deposition. The lasing occurs near 1.28 eV, while the wetting layer luminescence peaks at 1.43 eV. The dot size was selected to have only one electron and one hole level in the QD. The threshold current density equals to 80 Å cm^{-2} (80 K) and the characteristic temperature equals to 425 K in the temperature range 40–100 K for the resonator cavity length of 1.5 mm. At higher temperatures evaporation of carriers from dots starts resulting in a decrease in the maximal gain and in corresponding increase in the threshold current density (up to 2–3 kA cm^{-2}). To increase the gain one needs either to reduce the width of the PL line while maintaining the dot density, or to increase the dot density for the same size dispersion. The former is possible via careful optimization of growth parameters. The latter is possible via growth of vertically coupled quantum dots [see Fig. 1(d,e)]. The radiative lifetime decreases from 1.5 ns for quantum dots formed by a single-cycle 5 Å InAs deposition to 0.7 ns for the structure formed by a two period 5 Å InAs–15 Å GaAs–5 Å InAs deposition and to 0.4 ns for dots formed by a three-period 5 Å InAs–15 Å GaAs deposition. The PL peak shifts towards lower photon energies with increase in the number of deposition cycles. The PL intensity saturates at much higher excitation density in this case as well.

QD laser fabrication has also been realized using InGaAs quantum dots formed by deposition at 450°C resulting in a very dense ($\sim 3 \cdot 10^{11}$ cm^{-2}) array of small (~60 Å) uniform dots [see Fig. 6(b), insert, and [52]]. For this dot size, the electron wavefunction strongly penetrates in GaAs barrier regions[35] providing a significantly larger "effective" optical confinement factor. In Fig. 6(a), we show the temperature dependence of the lasing transition energy. The energy of the wetting layer emission and the GaAs barrier bandgap energy are shown for comparison. The lasing spectrum at RT and plan view TEM image are shown in Fig. 6(b).

Both the InAs and InGaAs QD lasers have demonstrated several important results[52]:

(i) High temperature stability and low threshold current density operation (80–120 Å cm^{-2}) in a broad temperature range (70–150 K). The characteristic temperature in this temperature range (T_0 = 350–425 K) significantly exceeds the theoretical limit for a QW laser.

(ii) Single longitudinal mode lasing is observed both at low and at high (300 K) temperatures for the InGaAs QD laser.

(iii) Quantum dot electroluminescence recorded from the edge of the structure is significantly depolarized (50% TE).

Injection lasers are realized also by stacking submonolayer InAs islands (see Fig. 2, insert), separating

them by thin GaAs regions. We have grown a submonolayer InAs-GaAs structure composed of 1 Å InAs and 6 Å GaAs layers repeated 14 times, introduced to a conventional GRIN SCH AlGaAs-GaAs laser. In Fig. 6(c) we show polarized electroluminescence (EL) recorded from the cleavage plane, EL polarization spectra (ρ), $\rho = (I^{TE} - I^{TM})/(I^{TE} + I^{TM})$, and PL spectrum recorded from the top of the structure. The resulting "submonolayer alloy" (SMA) structure differs significantly from conventional alloy (CA) InGaAs QW of the same average indium composition and thickness. Contrary to reference CA InGaAs QW structures grown under similar growth conditions where the heavy-hole exciton peak is *completely* TE polarized, a significant depolarization of the ground state heavy hole exciton emission in SMA lasers (40% TE) is manifested in Fig. 6(c).

An important result displayed in Fig. 6(c,d) is a remarkably small separation between light and heavy hole exciton peaks (~40 meV). For CA InGaAs QW of the same average width and In composition, this separation is about 70–75 meV in agreement with

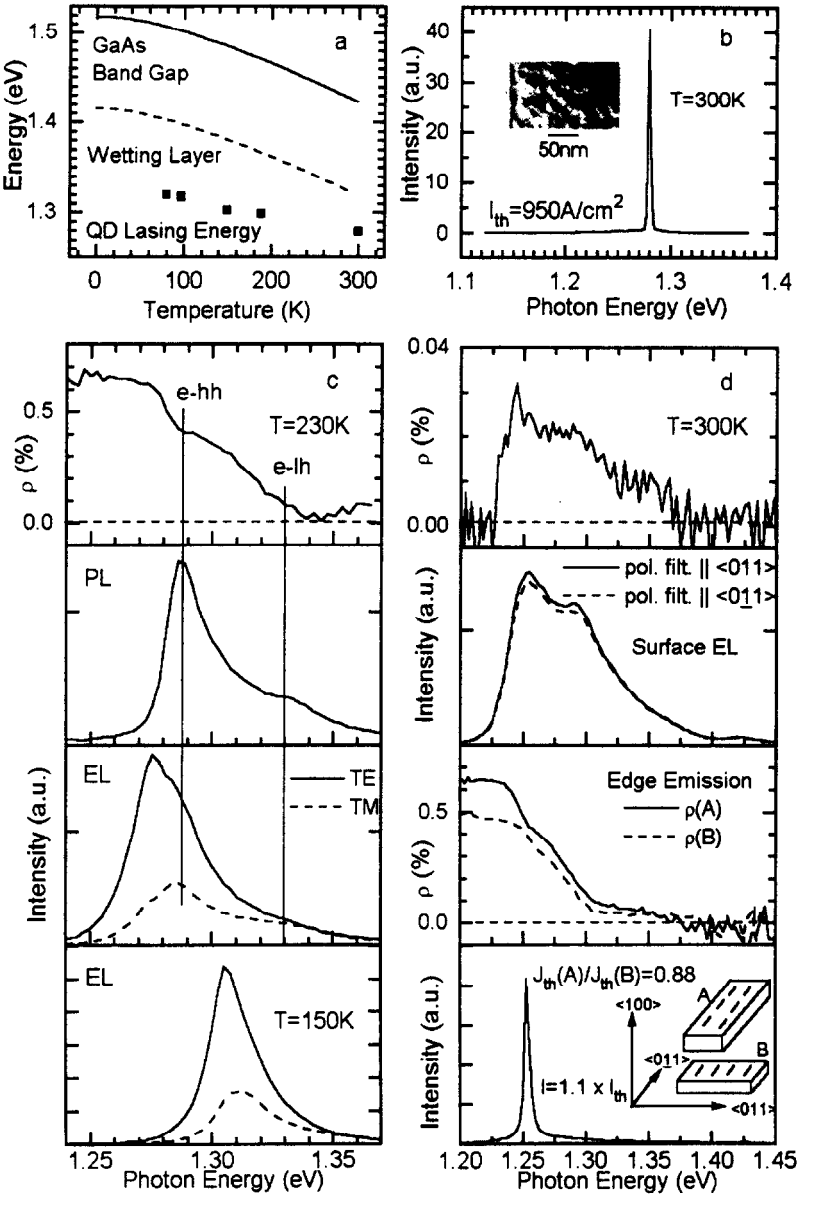

Fig. 6. (a) Lasing energy vs observation temperature for InGaAs quantum dot laser. Energy shifts of the InGaAs wetting layer luminescence and of GaAs bandgap are shown for comparison. (b) Room-temperature lasing spectrum. Plan-view TEM image is shown in the insert. (c) Linear polarization (ρ) of the edge electroluminescence of submonolayer alloy laser, $\rho = (I^{TE} - I^{TM})/(I^{TE} + I^{TM})$, PL spectrum from the top of the structure, polarized EL spectra at different temperatures. Not strong depolarization of edge emission. (d) Linear polarization of the surface EL recorded via window in the top contact; polarized surface EL spectra; directional anisotropy of the edge emission for two different stripe orientations (see insert) and lasing spectrum of the SMA alloy laser.

theoretical calculations[54]. As the splitting between heavy and light holes is controlled mostly by the uniaxial component of the strain tensor, remarkable reduction of this splitting indicates that holes are localized in regions with predominantly hydrostatic strain[35,51]. The PL linewidth at low temperatures (FWHM) is only ~ 5 meV excluding any nonuniform mesoscopic clusters, but in agreement with formation of well-ordered arrays of uniform InAs islands. The radiative lifetime measured in time resolved PL at 30 K is 250 ps, being much less than in a conventional alloy InGaAs QW (~ 1 ns).

EL recorded from a window in the top contact layer [see Fig. 6(d)] shows small *in plane* anisotropy [Fig. 6(d), top]. The HH exciton peak is weakly polarized in the direction *perpendicular* to the wires. This anisotropy agrees with the anisotropic strain directed along the InAs wire-like islands[19]. We have found a difference in the polarization of edge emission when the stripe is oriented along the wires and perpendicular to them. Depolarization is more pronounced when the stripe is oriented perpendicular to the wires and there is a finite *in plane* uniaxial strain directed parallel to the laser facet.

Lasing spectrum at RT is shown in Fig. 6(d), bottom. Anisotropy of the threshold current density for the two stripe orientations is observed, $J_{th}(A)/J_{th}(B) = 0.88$ [see Fig. 6(d)]. Threshold current density is lower when the stripe is oriented parallel to wires in agreement with the waveguide orientation anisotropy and equals to 120 A cm^{-2} (300 K, shallow mesa geometry) for 40 μm stripe width and 1500 μm cavity length.

We have shown that laterally and vertically ordered arrays of equisized and equishaped quantum dots can be directly formed in a single-crystalline matrix. These artificial three-dimensional crystals can be used in different devices: light emitters, light modulators, far-infrared detectors, resonant tunnelling structures, etc. Successful realization of quantum dot injection laser with ultrahigh temperature stability of threshold current has been demonstrated in this work which indicates the high importance of quantum dot arrays.

Acknowledgements—Parts of this work are supported by Volkswagen-Stiftung, by INTAS-94-1028 grant and by Deutsche Fortschungsgemeinschaft in the framework of Sfb 296. N.N.L. is grateful to Alexander von Humboldt Foundation.

REFERENCES

1. A. F. Andreev, *Zh. Eksp. Teor. Fiz.* **80,** 2042 (1981)—*Sov. Phys. JETP* **53,** 1063 (1981).
2. V. I. Marchenko, *Zh. Eksp. Teor. Fiz.* **81,** 1141 (1981)—*Sov. Phys. JETP* **54,** 605 (1981); V. I. Marchenko and A. Ya. Parshin, *Zh. Eksp. Teor. Fiz.* **79,** 257 (1980)—*Sov. Phys. JETP* **52,** 129 (1980).
3. V. I. Marchenko, *Pis'ma Zh. Eksp. Teor. Fiz.* **33,** 397 (1981)—*JETP Lett.* **33,** 381 (1981).
4. R. Nötzel, N. N. Ledentsov, L. Däweritz, M. Hohenstein and K. Ploog, *Phys. Rev. Lett.* **67,** 3812 (1991).
5. J. Tersoff and R. M. Tromp, *Phys. Rev. Lett.* **70,** 2782 (1993).
6. L. Goldstein, F. Glas, J. Y. Marzin, M. N. Charasse and G. Le Roux, *Appl. Phys. Lett.* **47,** 1099 (1985).
7. D. Leonard, M. Krishnamurthy, C. M. Reaves, S. P. Denbaars and P. M. Petroff, *Appl. Phys. Lett.* **63,** 3203 (1993); J. M. Moison, F. Houzay, F. Barthe, L. Leprice, E. Andre and O. Vatel, *Appl. Phys. Lett.* **64,** 196 (1994).
8. N. N. Ledentsov, M. Grundmann, N. Kirstaedter, J. Christen, R. Heitz, J. Böhrer, F. Heinrichsdorff, D. Bimberg, S. S. Ruvimov, P. Werner, U. Richter, U. Gösele, J. Heydenreich, V. M. Ustinov, A. Yu. Egorov, M. V. Maximov, P. S. Kop'ev and Zh. I. Alferov, *Proc. of the 22nd Int. Conf. on the Physics of Semiconductors*, Vancouver, Canada, 1994 (Edited by D. J. Lockwood), Vol. 3, p. 1855. World Scientific, Singapore (1995).
9. Y. Arakawa and H. Sakaki, *Appl. Phys. Lett.* **40,** 939 (1982).
10. Y. Arakawa and A. Yariv, *IEEE J. Quantum. Electron.* **QE22,** 1887 (1986).
11. H. Hibino, T. Fukuda, M. Suzuki, Y. Hommo, T. Sato, M. Iwatsuki, K. Miki and H. Tokumoto, *Phys. Rev. B* **47,** 13027 (1993).
12. M. Kasu and N. Kobayashi, *Appl. Phys. Lett.* **62,** 1262 (1993).
13. N. N. Ledentsov, G. M. Gur'yanov, G. E. Tsyrlin, V. N. Petrov, Yu. B. Samsonenko, A. O. Golubok and S. A. Tipisev, *Fiz. i Tekn. Poluprovodn.* **28,** 904 (1994); *Semiconductors* **28,** 526 (1994).
14. A. A. Baski and L. J. Whitman, *Phys. Rev. Lett.* **74,** 956 (1995).
15. G. M. Watson, D. Gibbs, D. M. Zehner, M. Yoon and S. G. J. Mohrie, *Phys. Rev. Lett.* **71,** 3166 (1993).
16. R. Koch, M. Borbonus, O. Haase and K. H. Rieder, *Phys. Rev. Lett.* **67,** 3416 (1991).
17. J. K. Zuo, R. J. Warmack, D. M. Zehner and J. F. Wendelken, *Phys. Rev. B* **47,** 10743 (1993).
18. V. A. Shchukin, A. I. Borovkov, N. N. Ledentsov and P. S. Kop'ev, *Phys. Rev. B* **51,** 10105 (1995); V. A. Shchukin, A. I. Borovkov, N. N. Ledentsov and D. Bimberg, *Phys. Rev. B* **51,** 17767 (1995).
19. P. D. Wang, N. N. Ledentsov, C. M. Sotomayor Torres, P. S. Kop'ev and V. M. Ustinov, *Appl. Phys. Lett.* **64,** 1526 (1994).
20. V. Bressler-Hill, A. Lorke, S. Varma, P. M. Petroff, K. Pond and W. H. Weinberg, *Phys. Rev. B* **50,** 8479 (1994).
21. Z. H. Ming, Y. L. Soo, S. Huang, Y. H. Kao, K. Stair, G. Devane and C. Choi-Feng, *Appl. Phys. Lett.* **66,** 165 (1995).
22. S. S. Ruvimov, P. Werner, K. Scheerschmidt, U. Gösele, J. Heydenreich, U. Richter, N. N. Ledentsov, M. Grundmann, D. Bimberg, V. M. Ustinov, A. Yu. Egorov, P. S. Kop'ev and Zh. I. Alferov, *Phys. Rev. B* **51,** 14766 (1995); Y. Androussi, A. Lefebvre, C. Delamarre, L. P. Wang, A. Dubon, B. Courbolès, C. Deparis and J. Massies, *Appl. Phys. Lett.* **66,** 3450 (1995).
23. G. M. Guryanov, G. E. Cirlin, V. N. Petrov, N. K. Polyakov, A. O. Golubok, S. Ya. Tipissev, E. P. Musikhina, V. B. Gubanov, Yu. B. Samsonenko and N. N. Ledentsov, *Surf. Sci.* (1995); G. E. Cirlin, G. M. Guryanov, A. O. Golubok, S. Ya. Tipissev, N. N. Ledentsov, P. S. Kop'ev, M. Grundmann and D. Bimberg, *Appl. Phys. Lett.* **67,** 97 (1995).
24. V. A. Shchukin, N. N. Ledentsov, P. S. Kop'ev and D. Bimberg, *Phys. Rev. Lett* **75,** 2968 (1995).
25. M. A. Grinfeld, *Dokl. Acad. Nauk SSSR* **290,** 1358 (1986); *Sov. Phys. Dokl.* **31,** 831 (1986).

26. M. Grundmann, N. N. Ledentsov, R. Heitz, L. Eckey, J. Christen, J. Böhrer, D. Bimberg, S. S. Ruvimov, P. Werner, U. Richter, U. Gösele, J. Heydenreich, V. M. Ustinov, A. Yu. Egorov, A. E. Zhukov, P. S. Kop'ev and Zh. I. Alferov, *Phys. Stat. Sol.* **188,** 249 (1995).
27. A. G. Khachaturyan, *Theory of Structural Transformations in Solids*. Wiley, New York (1983).
28. O. L. Alerhand, D. Vanderbilt, R. D. Meade and J. D. Joannopoulos, *Phys. Rev. Lett.* **61,** 1973 (1988); I. P. Ipatova, V. G. Malyshkin and V. A. Shchukin, *J. Appl. Phys.* **74,** 7198 (1993); *Phil. Mag. B* **70,** 557 (1994).
29. P. D. Wang, N. N. Ledentsov, C. M. Sotomayor Torres, P. S. Kop'ev and V. M. Ustinov, *Appl. Phys. Lett.* **66,** 112 (1995).
30. M. V. Belousov, N. N. Ledentsov, M. V. Maximov, P. D. Wang, I. N. Yassievich, N. N. Faleev, A. Kozin, V. M. Ustinov, P. S. Kop'ev and C. M. Sotomayor Torres, *Phys. Rev. B* **51,** 14346 (1995).
31. N. N. Ledentsov, P. D. Wang, C. M. Sotomayor Torres, A. Yu. Egorov, M. V. Maximov, V. M. Ustinov, A. E. Zhukov and P. S. Kop'ev, *Phys. Rev. B* **50,** 12171 (1994).
32. S. S. Ruvimov, P. Werner, K. Scheerschmidt, U. Richter, U. Gösele, J. Heydenreich, N. N. Ledentsov, M. Grundmann, D. Bimberg, V. M. Ustinov, A. Yu. Egorov, P. S. Kop'ev and Zh. I. Alferov, *Inst. Conf. Phys. Ser.* The Institute of Physics, Bristol (1995) (in press).
33. A. Madhukar, Q. Xie, P. Chen and A. Koknar, *Appl. Phys. Lett.* **64,** 2727 (1994).
34. E. Tournié, A. Trampert and K. Ploog, *Europhysics Lett.* **25,** 663 (1994); A. Trampert, E. Tournié and K. H. Ploog, *Phys. St. Solid* **145,** 481 (1994).
35. M. Grundmann, in: *Adv. Solid St. Phys.* **35,** 123 (1996); M. Grundmann, O. Stier and D. Bimberg, *Phys. Rev. B* **51** 11969 (1995).
36. M. Grundmann, J. Christen, N. N. Ledentsov, J. Böhrer, D. Bimberg, S. S. Ruvimov, P. Werner, U. Richter, U. Gösele, J. Heydenreich, V. M. Ustinov, A. Yu. Egorov, A. E. Zhukov, P. S. Kop'ev and Zh. I. Alferov, *Phys. Rev. Lett.* **74,** 4043 (1995).
37. N. N. Ledentsov, M. V. Maximov, P. S. Kop'ev, V. M. Ustinov, M. V. Belousov, B. Ya. Meltser, S. V. Ivanov, V. A. Shchukin, Zh. I. Alferov, M. Grundmann, D. Bimberg, S. S. Ruvimov, U. Richter, P. Werner, U. Gösele, U. Heydenreich, P. D. Wang and C. M. Sotomayor Torres, *J. Microelectron.* **26,** 871 (1995).
38. R. Heitz, N. N. Ledentsov, M. Grundmann, L. Eckey, D. Bimberg, V. M. Ustinov, A. Yu. Egorov, A. E. Zhukov, P. S. Kop'ev and Zh. I. Alferov *Appl. Phys. Lett.* **68,** 361 (1996).
39. E. I. Rashba, *Fiz. Tekn. Poluprovodn.* **8,** 1241 (1974); *Sov. Phys. Semicond.* **8,** 807 (1974).
40. P. D. Wang, N. N. Ledentsov, C. M. Sotomayor Torres, I. N. Yassievich, A. Pakhomov, A. Yu. Egorov, P. S. Kop'ev and V. M. Ustinov, *Phys. Rev. B* **50,** 1604 (1994).
41. S. Permogorov, *Phys. St. Sol.* **68,** 9 (1975).
42. R. P. Stanley, J. Hegarty, R. Fisher, J. Feldman, E. O. Göbel, R. D. Feldman and R. F. Austin, *Phys. Rev. Lett.* **67,** 128 (1991).
43. N. N. Ledentsov, R. Nötzel, P. S. Kop'ev and K. Ploog, *Appl. Phys.* **A55,** 533 (1992).
44. R. Nötzel, N. N. Ledentsov, L. Däweritz, K. Ploog and M. Hohenstein, *Phys. Rev. B* **45,** 3507 (1992).
45. R. Nötzel, N. N. Ledentsov and K. Ploog, *Phys. Rev. B* **47,** 1299 (1993).
46. N. N. Ledentsov, S. V. Ivanov, M. V. Maximov, I. V. Sedova, I. G. Tabatadze and P. S. Kop'ev, *Semiconductors* **29,** 34 (1995).
47. P. D. Wang and C. M. Sotomayor Torres, *J. Appl. Phys.* **74,** 5047 (1993).
48. H. Benisty, C. M. Sotomayor Torres and C. Weisbuch, *Phys. Rev. B* **44,** 10945 (1991); T. Inoshita and H. Sakaki, *Phys. Rev. B* **46,** 7260 (1992).
49. D. N. Mirlin, A. A. Sirenko and R. Planel, *Solid St. Commun.* **91,** 545 (1994).
50. P. S. Kop'ev, D. N. Mirlin, V. F. Sapega, A. A. Sirenko, *JETP Lett.* **51,** 708 (1990); D. N. Mirlin, P. S. Kop'ev, I. I. Reshina, V. F. Sapega and A. A. Sirenko, *Proc. 20th Int. Conf. on the Physics of Semiconductors* (Edited by E. M. Anastassakis, J. D. Joannopoulos), Vol. 2, p. 1037. World Scientific, Singapore (1990).
51. M. Grundmann, N. N. Ledentsov, O. Stier, D. Bimberg, V. M. Ustinov, P. S. Kop'ev and Zh. I. Alferov *Appl. Phys. Lett.* **68,** 979 (1996)
52. N. Kirstaedter, N. N. Ledentsov, M. Grundmann, D. Bimberg, U. Richter, S. S. Ruvimov, P. Werner, J. Heydenreich, V. M. Ustinov, M. V. Maximov, P. S. Kop'ev and Zh. I. Alferov, *Electron. Lett.* **30,** 1416 (1994).
53. H. Temkin, N. K. Dutta, T. Tanbun-Ek, R. A. Logan and A. M. Sergent, *Appl. Phys. Lett.* **57,** 1610 (1990).
54. M. P. Houng, *Superlatt. Microstruct.* **6,** 421 (1989).